We are IntechOpen, the world's leading publisher of Open Access books Built by scientists, for scientists

4,800
Open access books available

122,000
International authors and editors

135M
Downloads

Our authors are among the

154
Countries delivered to

TOP 1%
most cited scientists

12.2%
Contributors from top 500 universities

CLARIVATE ANALYTICS BOOK CITATION INDEX INDEXED

WEB OF SCIENCE™

Selection of our books indexed in the Book Citation Index in Web of Science™ Core Collection (BKCI)

Interested in publishing with us?
Contact book.department@intechopen.com

Numbers displayed above are based on latest data collected.
For more information visit www.intechopen.com

Chapter

Mechanism, Model, and Upscaling of the Gas Flow in Shale Matrix: Revisit

Zhiming Hu, Yaxiong Li and Yanran Li

Abstract

Shale gas accounts for an increasing proportion in the world's oil and gas supply, with the properties of low carbon, clean production, and huge potential for the compensation for the gradually depleted conventional resources. Due to the ubiquitous nanopores in shale matrix, the nanoscale gas flow becomes one of the most vital themes that are directly related to the formulation of shale gas development schemes, including the optimization of hydraulic fracturing, horizontal well spacing, etc. With regard to the gas flow in shale matrix, no commonly accepted consensus has been reached about the flow mechanisms to be considered, the coupled flow model in nanopores, and the upscaling method for its macroscopic form. In this chapter, the propositions of wall-associated diffusion, a physically sound flow mechanism scheme, a new coupled flow model in nanopores, the upscaling form of the proposed model, and the translation of lab-scale results into field-scale ones aim to solve the aforementioned issues. It is expected that this work will contribute to a deeper understanding of the intrinsic relationship among various flow mechanisms and the extension of the flow model to full flow regimes and to upscaling shale matrix, thus establishing a unified model for better guiding shale gas development.

Keywords: shale gas, diffusion, viscous flow, coupling coefficient, generalized model, pore size distribution, macroscopic form

1. Introduction

Shale gas refers to a kind of self-generating and self-preserving natural gas, which gathers mainly in a free or adsorbed state in the organic-rich dark shale or high-carbon mud shale [1]. With vast reserves and the potential to offset the gradually depleted conventional resources worldwide and cut down carbon emissions at the same time, shale gas is playing an increasingly important role in ensuring global energy safety. Because shale matrix is characterized by various nanopores, where the gas flow is of high nonlinearity and complexity, an in-depth study of the mathematical model for the gas flow capacity in shale matrix is in urgent demand.

The mechanisms considered in different literature are listed in **Table 1**. It is obvious that opinions vary greatly on the flow mechanism scheme applied. The noteworthy aspects include the following: what the relationship among the various

Literature	Mechanisms considered
Klinkenberg [2]	Slip flow
Javadpour [3], Haghshenas et al. [4], Wu et al. [5], Sun et al. [6]	Knudsen diffusion and slippage
Veltzke and Thöming [7]	Viscous flow and Knudsen diffusion
Li et al. [8]	Continuum flow, slip flow, transition flow, and free molecular flow
Mi et al. [9]	Diffusion and slippage, where the form of diffusion varies according to the Knudsen number range, including Fick diffusion, transitional diffusion, and Knudsen diffusion
Song et al. [10]	Viscous flow, Knudsen diffusion, and surface diffusion, with surface diffusion not considered for inorganic pores

Table 1.
Different flow mechanism schemes in literature.

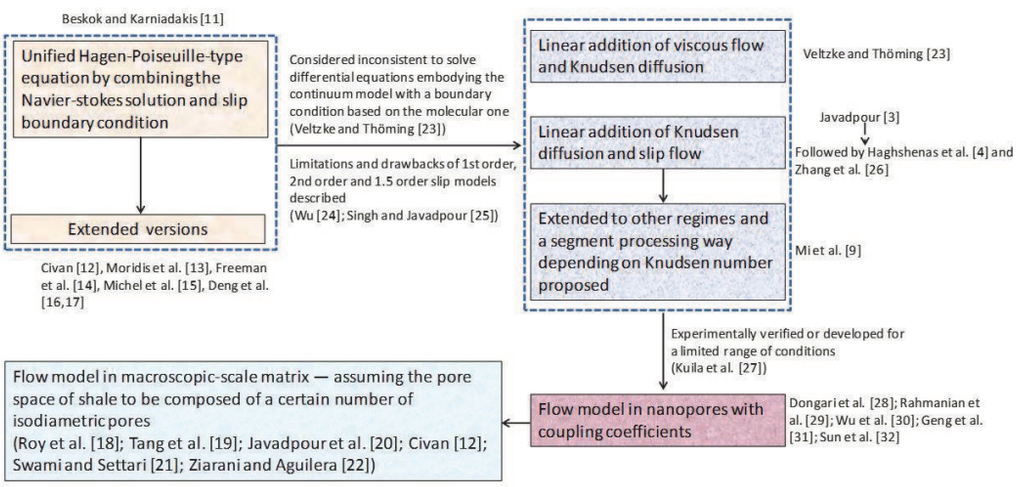

Figure 1.
A brief summary of the common methodology used in different research [11, 13, 14, 16, 17, 23–26, 28, 32].

flow mechanisms of shale gas, e.g., slippage, Fick diffusion, Knudsen diffusion, etc., is; whether there is a repeated superposition of these mechanisms for specific flow calculation; and how to deal with the relationship among the various flow mechanisms, etc. There is no clear answer to these problems in current literature.

Figure 1 shows the common research methodology of the flow models used in different literature. It indicates that because the method of the continuum model with a boundary condition based on the molecular one is considered inconsistent and the limitations and drawbacks of first-order, second-order, and 1.5-order slip models are described, some studies, which are listed in **Figure 1**, are inclined to add related flow mechanisms linearly. Furthermore, the mathematical models of viscous flow and various types of diffusion do not fully agree with common flow cognition as these theories and models were experimentally verified or developed for a limited range of conditions [27]. For this reason, coupling coefficients are introduced to rectify this kind of limitation, so as to enhance the correspondence between the flow model and Knudsen number (Kn). Finally, because the secondhand average method, e.g., assuming the pore space of shale to be composed of a certain number of isodiametric pores regardless of the pore size distribution, is widely used in the research of shale gas flow, more explicit means, like taking the existence of various pore sizes in shale into account, should be adopted for transforming the flow model in nanopores to that in macroscopic-scale shale matrix.

Based on the literature survey for shale gas flow in shale matrix, we know that the flow mechanism scheme with its corresponding coupling method is very crucial and has not yet been solved. In addition, although the integration method using specific functions has been proposed to facilitate the consideration of various pore sizes in shale matrix, real shale experiments are rarely involved to realize this point with definitely determined parameters.

Firstly, in this chapter, the concept of wall-associated diffusion is presented to clarify the relationship between slippage effect and several types of diffusion. Secondly, a physically sound flow mechanism scheme, which considers both division of mechanical mechanisms in nanopores and partition of flow space, has been proposed by virtue of the proposition of wall-associated diffusion. Thirdly, the coupling coefficients corresponding to the flow mechanisms considered are deduced to comply with the basic flow regime cognition, so as to establish a new coupled flow model in nanopores. Fourthly, the pore size distribution experiments for real shale samples from a gas field are utilized to realize the upscaling transformation of the flow model in nanopores into that in the macroscopic-scale shale matrix, with definitely determined fitting parameters for the establishment of a unified model for the gas flow prediction in shale matrix. Finally, a case study is presented to show how the lab-scale results are translated into field-scale ones.

2. Flow mechanisms in gas-shale matrix

There are many types of flow mechanisms in shale matrix, including slippage effect, Fick diffusion, transition diffusion, Knudsen diffusion, surface diffusion, etc. It can be seen from the literature survey in Section 1 that different flow mechanism schemes have formed aiming at establishing a calculation model to properly characterize the nanoscale shale gas flow. There may be views that the more flow mechanisms are taken into account, the more precise the established models are. However, this is not the opinion in this chapter.

As is known, Klinkenberg [33] first discovered in 1941 the phenomenon that, when measuring the gas permeability of rock, not only the measurement result is higher than the liquid measurement value but also it has strong pressure dependence and attributed it to the slippage behavior of gas in the rock pores. Specifically, gas slippage refers to the phenomenon that the near-wall gas molecules move relative to the wall surface when flowing through the medium channels [34]. In essence, the gas slip flow results from the interaction of gas molecules and pore walls, so the gas molecules in the vicinity of walls are in motion and contribute an additional flux, which is macroscopically characterized by the non-zero gas velocities on channel walls, thus resulting in slip flow [35, 36]. The jump model assumes that the adsorbed gas molecules jump from one adsorption site to the adjacent adsorption site on the pore surface, which is considered to be suitable for the research on the surface diffusion of the adsorbed gas in shale nanopores [37]. Meanwhile, when the molecular mean free path is obviously larger than the pore diameter, the gas-wall collision dominates, and the collision between gas molecules is secondary, which is characterized by Knudsen diffusion [9, 38, 39].

In brief, both Knudsen diffusion and surface diffusion lead to non-zero moving speeds of the gas molecules around walls. Furthermore, from the viewpoint of microscopic motion mechanisms, they are both related to gas–solid interactions, which is consistent with slippage phenomenon in essence. Therefore, a new concept named “wall-associated diffusion” [40] is proposed, which characterizes the overall role of surface diffusion and Knudsen diffusion, as shown in **Figure 2**.

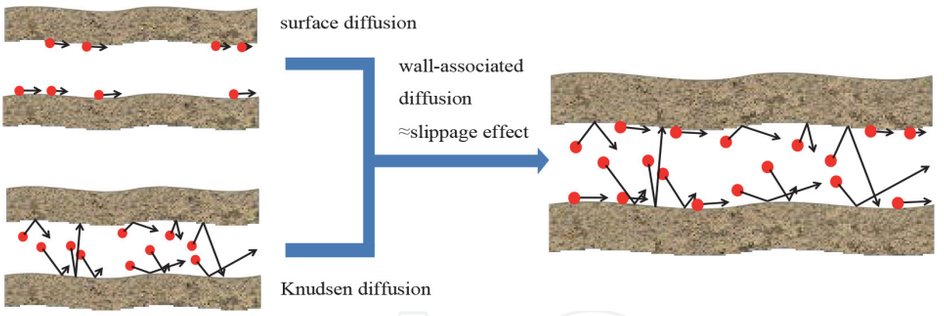

Figure 2.
Relationship between wall-associated diffusion and slippage effect [40].

The proposition of wall-associated diffusion has practical significance and multiple research significance as follows [40].

To begin with, in terms of mechanical mechanisms, since wall-associated diffusion describes the diffusion mechanisms of shale gas related to gas-wall interactions, it bridges the relationship between slippage effect and several types of diffusion, which prevents reduplicated superposition of shale gas flow mechanisms in nanoscale pores. This is where the practical significance lies. Besides, wall-associated diffusion can be regarded as a detailed form of slippage effect, dividing slippage effect into two distinct parts, i.e., surface diffusion and Knudsen diffusion. The two parts differ obviously in their mechanical mechanisms and motion patterns. Accordingly, the research significance of wall-associated diffusion involves not only the function of morphological descriptions but also the possibility of slip phenomenon research by different mechanical mechanisms. Lastly, another research significance is that wall-associated diffusion breaks through the limitation that the concept of slippage does not apply for high Knudsen number, with, however, the fact that wall effects still contribute to gas flow for high Knudsen number. Therefore, in extremely small nanopores, for example, where slip flow regime is not applicable, the wall-associated diffusion derived from physical morphology can well be used to explore the so-called slip phenomenon in other flow regimes apart from slip flow regime.

By virtue of the concept of wall-associated diffusion, the flow mechanism scheme used in this work is to be discussed next.

There is no doubt that all the mechanisms, such as continuum flow, slip flow, Knudsen diffusion, bulk diffusion, etc., have been studied in previous literature for the exploration of shale gas flow. However, it is a determinative flow mechanism scheme that is vital. According to the literature survey, apart from combining the Navier-Stokes solution with slip boundary condition whose deficiency has been mentioned in Section 1, there is also a trend in literature to assume a combination of certain flow mechanisms and check the consistency of the model results with experimental data. This method is favorable from an engineering point of view but meanwhile leads to the status that coincidence often exists and no commonly accepted consensus has formed currently. In this work, we discuss the issue physically. Firstly, due to the multiple advantages of wall-associated diffusion over the concept of slippage effect, slippage effect is replaced with wall-associated diffusion in the following discussion. On the one hand, the flow space in nanopores can be divided into two parts: the bulk phase region and the Knudsen layer [41]. On the other hand, the microscopic mechanical mechanisms can be divided into the gas–gas and gas-wall interactions. If a new comprehensive flow scheme, including viscous flow and bulk diffusion which belong to bulk phase flow and surface diffusion and Knudsen diffusion which are associated with gas-wall interactions causing non-zero flow velocities near pore walls, is proposed, the considerations of the division of flow space and mechanical mechanisms can be both realized.

It should be noted that with the help of the methodology applied here, some flow mechanisms that are easily omitted are now included, such as bulk diffusion, an important diffusion process which is controlled by a mechanical mechanism obviously different from Knudsen diffusion. Furthermore, because the individual flow expressions, e.g., those for viscous flow and diffusion, were experimentally verified or developed for a limited range of conditions [27], the proposed physical flow mechanism scheme avoids unnecessary attempts to fit the mathematical models to experimental data so as to determine which flow mechanisms should be considered, laying a solid foundation for the research on the coupled flow model in nanopores discussed below.

To conclude, taking both division of mechanical mechanisms in nanopores and partition of flow space into account, viscous flow and bulk diffusion, which belong to bulk phase flow and result from gas–gas interactions, and surface diffusion and Knudsen diffusion, which are associated with gas-solid interactions and result in non-zero flow velocities near pore walls, are included in the proposed flow mechanism scheme.

3. Coupled model of shale gas flow in nanopores

Based on the flow scheme proposed in Section 2, the flow mechanisms considered include viscous flow, bulk diffusion, surface diffusion, and Knudsen diffusion. Considering the influence of adsorption layers, in which the system is assumed to reach dynamic adsorption equilibrium state instantaneously, the mass flow of the four mechanisms can be expressed, respectively, as:

$$N_D = -\frac{10^{-36}\pi\rho_{avg}}{8\mu}\left(r_{in} - \frac{pd_m}{p_L + p}\right)^4 \frac{\mathrm{d}p}{\mathrm{d}l} \tag{1}$$

$$N_b = N_F = -\frac{10^{-9} M k_B}{3R\mu d_m}\left(r_{in} - \frac{pd_m}{p_L + p}\right)^2 \frac{\mathrm{d}p}{\mathrm{d}l} \tag{2}$$

$$N_K = -\frac{2\times 10^{-27}}{3}\left(\frac{8\pi M}{RT}\right)^{0.5}\left(r_{in} - \frac{pd_m}{p_L + p}\right)^3 \frac{\mathrm{d}p}{\mathrm{d}l} \tag{3}$$

$$N_s = -0.016\times 10^{-22}\times \exp\left(-\frac{0.45q}{RT}\right)\frac{\rho_s M}{pV_{std}}\frac{q_L p}{p_L + p}\cdot\frac{1-\phi_{co}}{\phi_{co}}\pi {r_{in}}^2\frac{\mathrm{d}p}{\mathrm{d}l} \tag{4}$$

where N_D = viscous mass flow in a pipe, kg·s^{-1}.
N_b = mass flow of bulk diffusion, kg·s^{-1}.
N_F = mass flow of Fick diffusion, kg·s^{-1}.
N_K = mass flow of Knudsen diffusion, kg·s^{-1}.
N_s = mass flow of surface diffusion, kg·s^{-1}.
r_{in} = inner radius of a pipe, nm.
ρ_{avg} = density of gas at average pressure of inlet and outlet, kg·m^{-3}.
μ = gas viscosity, Pa·s.
d_m = diameter of gas molecules, nm.
p_L = Langmuir pressure, Pa.
$\mathrm{d}p/\mathrm{d}l$ = pressure gradient, Pa·m^{-1}.
M = molecular weight, kg·mol^{-1}.
R = universal gas constant, =8.314 J·mol^{-1}·K^{-1}.
k_B = Boltzmann constant, =1.38 × 10^{-23} J·K^{-1}.
T = ambient temperature, K.

ρ_s = density of shale matrix, kg·m^{-3}.
V_{std} = molar volume of gas under standard conditions, m^3·mol^{-1}.
q_L = Langmuir volume, m^3·kg^{-1}.
Φ_{co} = porosity of a core sample, dimensionless.

The expression of Fick diffusion (2) is referred to as bulk diffusion and represented by N_b.

The case study in literature [42] shows that although the equations of viscous flow and diffusion already contain variables varying with temperature, pressure, and other factors, they make sense within only a certain range of flow regimes and deviate from the actual situation within other range that is not taken into account. Introducing coupling coefficients to different flow mechanisms can help modify the correspondence between the mathematical models (i.e., those of viscous flow and diffusion) and Knudsen number and establish generalized models without segment processing as Kn varies.

In contrast to the coupling coefficients reported in published literatures [29, 31, 43, 44], the derivation of new coupling coefficients corresponding to the proposed flow mechanism scheme is performed, and the coupling coefficient of one certain flow mechanism will not be optionally set as 100%. The coupling coefficients of viscous flow, bulk diffusion, Knudsen diffusion, and surface diffusion are represented by $f_1(\mathrm{Kn})$, $f_2(\mathrm{Kn})$, $f_3(\mathrm{Kn})$, and $f_4(\mathrm{Kn})$ respectively, which are the functions of Kn. The expressions of the coupling coefficients are set according to the characteristics of flow regimes, where the following assumptions are used:

1. Let $f_1(\mathrm{Kn}) + f_2(\mathrm{Kn}) = 1/(1 + \mathrm{Kn})$ and $f_3(\mathrm{Kn}) + f_4(\mathrm{Kn}) = \mathrm{Kn}/(1 + \mathrm{Kn})$ based on the molecular collision theory that the ratio of collision frequency between molecules to total collision frequency and that of molecule-wall collision frequency to total collision frequency are $1/(1 + \mathrm{Kn})$ and $\mathrm{Kn}/(1 + \mathrm{Kn})$, respectively [30].

2. When Kn equals to 0, only viscous flow is assumed to exist [45], i.e., $f_1(\mathrm{Kn}) = 1$ and $f_2(\mathrm{Kn}) = f_3(\mathrm{Kn}) = f_4(\mathrm{Kn}) = 0$.

3. It is transition flow when $10^{-1} < \mathrm{Kn} < 10$, and several diffusion processes play roles at the same time ([31, 46]; thus, $f_1(\mathrm{Kn})$ is assumed to be negligible at the logarithmic median of this range ([29, 43]), i.e., $f_1(\mathrm{Kn})$ is close to 0 when $\mathrm{Kn} > 1$.

4. As Kn approaches to 0 or is sufficiently large, $f_2(\mathrm{Kn})$ is close to 0.

5. $f_3(\mathrm{Kn})$ is small when $\mathrm{Kn} < 1$ and increases significantly when $\mathrm{Kn} > 1$, until close to 1 in the range of $\mathrm{Kn} > 10$ [29, 43].

6. In the whole range of flow regimes, $f_1(\mathrm{Kn})$, $f_2(\mathrm{Kn})$, $f_3(\mathrm{Kn})$, and $f_4(\mathrm{Kn})$ should all be nonnegative and change smoothly with Kn to embody the gradual evolvement of the flow as the condition varies.

Based on the above narrations, it physically defines that $f_1(\mathrm{Kn}) = \mathrm{e}^{-\alpha \mathrm{Kn}}$, $f_2(\mathrm{Kn}) = 1/(1 + \mathrm{Kn}) - \mathrm{e}^{-\alpha \mathrm{Kn}}$, $f_3(\mathrm{Kn}) = \mathrm{e}^{-\beta/\mathrm{Kn}}$, and $f_4(\mathrm{Kn}) = \mathrm{Kn}/(1 + \mathrm{Kn}) - \mathrm{e}^{-\beta/\mathrm{Kn}}$, where α and β are dimensionless constants determining the bump levels of the variation curves. α and β are set as 5 and 1.8 [42], respectively, to further realize the compliance of the coupling coefficients with the narrated flow regime characteristics.

Hence, the mass flow in nanopores can be expressed as:

$$N = e^{-5\mathrm{Kn}}N_D + \left(\frac{1}{1+\mathrm{Kn}} - e^{-5\mathrm{Kn}}\right)N_b + e^{-1.8/\mathrm{Kn}}N_K + \left(\frac{\mathrm{Kn}}{1+\mathrm{Kn}} - e^{-1.8/\mathrm{Kn}}\right)N_s \quad (5)$$

where N = mass flow in a pipe, $\mathrm{kg{\cdot}s^{-1}}$.

The variation curves of the four coupling coefficients and $f_1(\mathrm{Kn}) \times N_D$, $f_2(\mathrm{Kn}) \times N_b$, $f_3(\mathrm{Kn}) \times N_K$, and $f_4(\mathrm{Kn}) \times N_s$ with Kn are depicted in **Figures 3** and **4** [42].

The benefits of introducing the above coupling coefficients to viscous flow and diffusion are significant:

1. It is clear that because $f_1(\mathrm{Kn}), f_2(\mathrm{Kn}), f_3(\mathrm{Kn})$, and $f_4(\mathrm{Kn})$ are all nonnegative, the segment processing of mathematical models can be avoided, i.e., Eq. (5) can be uniformly used for the coupling calculation in the scope of $0 < \mathrm{Kn} < \infty$, without the need to change the functional forms by reason of the limited applicability of coupling coefficients.

2. Eq. (5) bridges the gaps between different flow regimes, i.e., the jumps of flow rates at the critical points between different regimes have vanished. Furthermore, the mathematical models are further constrained by virtue of the molecular collision theory to better reflect the basic flow regime knowledge.

3. Taking the viewpoints of Refs. [30, 32] as examples for comparison with this work, it should be noted that slip flow refers to the enhanced flow, including the part of original viscous flow and the other part called slippage effect which is represented by the non-zero velocities of the near-wall molecules due to gas-wall interactions. Therefore, it is more suitable to regard the ratio of gas–gas collision frequency to total collision frequency as the total coupling coefficient of viscous flow and bulk diffusion rather than that of the slip flow [30, 32].

4. The same examples [30, 32] are used for comparison. It is continuum flow when Kn approximates to 0. However, the coupling coefficient of slip flow is 1 when Kn = 0 in papers [30, 32], implying slip flow dominates in continuum flow regime, which contradicts the flow regime knowledge. This issue has been solved in this chapter.

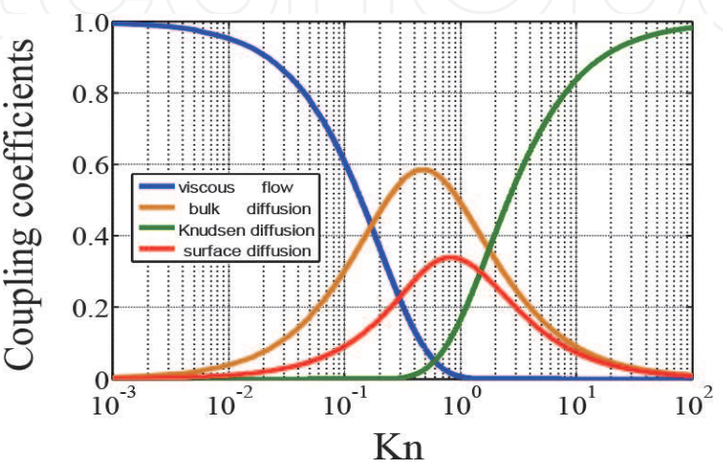

Figure 3.
Variation curves of the coupling coefficients (dimensionless) of viscous flow, bulk diffusion, Knudsen diffusion, and surface diffusion with Kn (dimensionless) [42].

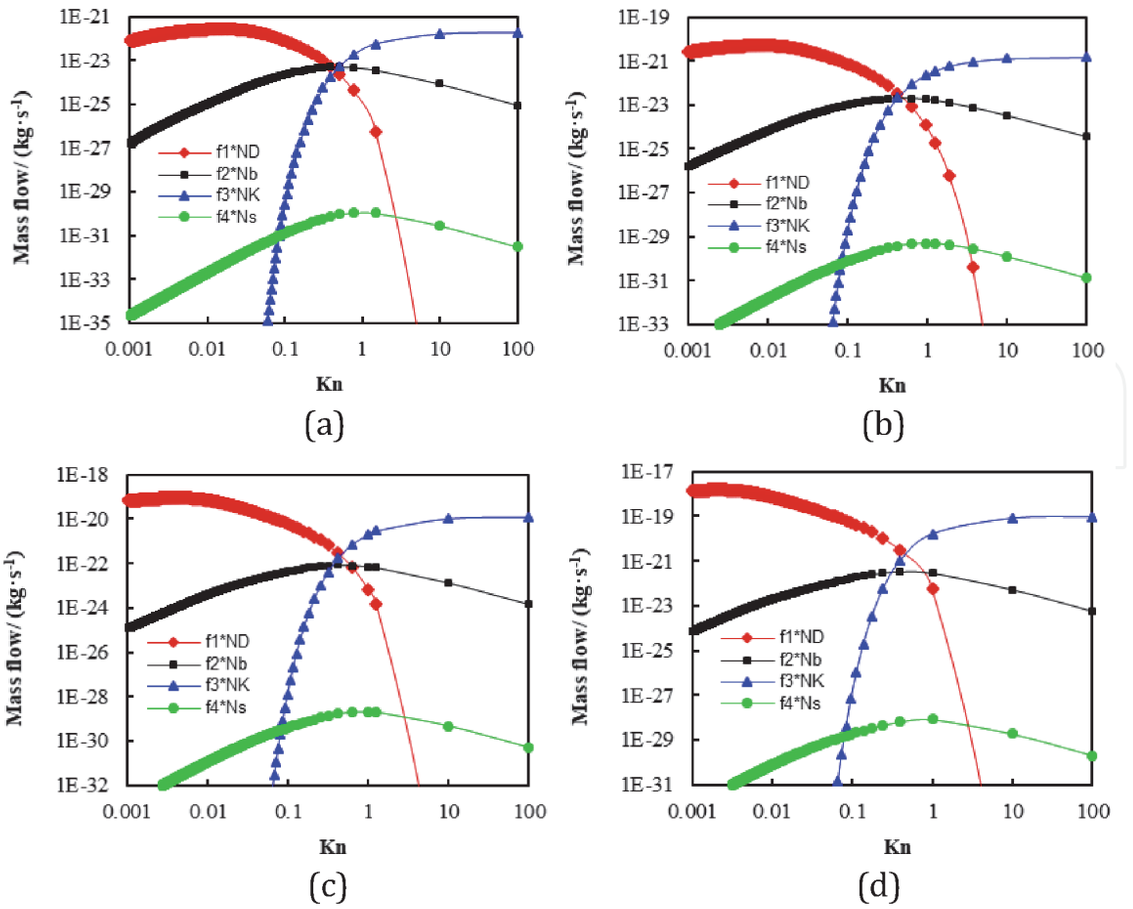

Figure 4.
Variations of viscous flow and diffusion with Kn (dimensionless) after introducing coupling coefficients for the gas flow in pores of (a) 5 nm, (b) 10 nm, (c) 20 nm, and (d) 40 nm at 353 K. f_1*N_D, f_2*N_b, f_3*N_K, and f_4*N_s denote the results of viscous flow, bulk diffusion, Knudsen diffusion, and surface diffusion, respectively [42].

4. Coupled mathematical model in macroscopic-scale shale matrix

In this section, the experimental results of full-scale pore size distributions of real shale samples from a gas field are combined with the coupled flow model in nanopores to realize the upscaling transformation of the flow model into that in macroscopic-scale shale matrix by integration.

In the unitary model which is widely used for the flow estimation on a macroscopic scale [12, 18–22], indirect averaging methods are applied, e.g., the pore space of shale is assumed to be composed of a certain number of isodiametric pores, regardless of the pore size distributions. Some research [15, 47] used specific functions to characterize the probability density function of shale pore size distributions, with, however, assumed parameters for the purpose of conducting parameter sensitivity analysis. Here, the fitting parameters needed for the macroscopic form of the derived coupled flow model in nanopores are obtained by performing the experiments of pore size distributions of real shale samples from a gas field.

Michel et al. [15] and Xiong et al. [47] described the probability density function of shale pore size distributions as logarithmic normal distribution. Enlightened by their studies, the following expression is used to fit the experimental data of full-scale shale pore size distributions:

$$f(r_{in}) = \frac{1}{r_{in}\sigma\sqrt{2\pi}} e^{-0.5\left(\frac{\ln r_{in}-\eta}{\sigma}\right)^2} \tag{6}$$

Samples	η/dimensionless	σ/dimensionless
Ning 203-219	0.9428	1.0890
Ning 203-240	1.3530	1.2100
Ning 203-250	0.1207	0.4189
Average	0.8055	0.9060

Table 2.
Fitting results of η and σ.

where η = normal mean, dimensionless.

σ = variance, dimensionless.

Three kinds of experiments, i.e., the high-pressure mercury intrusion experiment, the liquid nitrogen adsorption experiment, and the low-temperature carbon dioxide adsorption experiment, were performed, and the full-scale pore size distribution data of the three shale samples from the Well "Ning 203", Longmaxi formation of Changning-Weiyuan district, Sichuan Basin of China, were obtained by stitching the three results together according to the effective range of each experiment, where the total volume of pores greater than 100 nm is attributed to the pore whose radius is closest to 100 nm in the experiments allowing for the difficulty of curve fitting caused by the severe fluctuations of the pore size data [42]. The values of η and σ are listed in **Table 2**. Because the samples "Ning 203-219", "Ning 203-240", and "Ning 203-250" are all taken from a depth interval of 2300-2400 m, the three groups of data in **Table 2** are averaged, i.e., η = 0.8055 and σ = 0.9060, to represent the typical shale pore size distribution in this depth range.

The number of single pipes in shale with the radius range of r_{in} to r_{in} + dr_{in} is expressed in Eq. (7). By integrating in the entire pore size range, the flow rate in shale is obtained as Eq. (8):

$$\frac{10^{18}\phi_{co}V_{co}}{\pi {r_{in}}^2 L_{co}} f(r_{in})\mathrm{d}r_{in} \tag{7}$$

$$Q = \int_{r_{in,\min}}^{r_{in,\max}} \frac{10^{18} N \phi_{co} V_{co}}{\pi {r_{in}}^2 L_{co}} f(r_{in})\mathrm{d}r_{in} \tag{8}$$

where V_{co} = apparent volume of a core sample, m^3.

L_{co} = length of a core sample, m.

$r_{in,\min}$ = lower limit of integration, which should be larger than 0.19 nm because the diameter of methane molecules is 0.38 nm [48].

$r_{in,\max}$ = upper limit of integration.

The macroscopic-scale mathematical model of shale gas flow can be obtained by substituting Eqs. (5) and (6) into Eq. (8) as:

$$Q = \int_{r_{in,\min}}^{r_{in,\max}} \frac{10^{18}\left[e^{-5\mathrm{Kn}}N_D + \left(\frac{1}{1+\mathrm{Kn}} - e^{-5\mathrm{Kn}}\right)N_b + e^{-1.8/\mathrm{Kn}}N_K + \left(\frac{\mathrm{Kn}}{1+\mathrm{Kn}} - e^{-1.8/\mathrm{Kn}}\right)N_s\right]\phi_{co}V_{co}}{\pi {r_{in}}^3 L_{co}\sigma\sqrt{2\pi}} e^{-0.5\left(\frac{\ln r_{in}-\eta}{\sigma}\right)^2}\mathrm{d}r_{in} \tag{9}$$

Literature survey shows that there are several main upscaling methods of flow models from microscopic to macroscopic scale, i.e.:

Method (1): the commonly used unitary model [12, 18–22] as already mentioned.

Method (2): the sum method of calculating the permeability of every straight capillary tube [27].

Method	Description/equation	Advantages	Shortcomings
Unitary pipe model [12]	$q = nq_h = \frac{\phi A_b}{\pi {R_h}^2} q_h$ (q, total flow, $m^3 \cdot s^{-1}$; n, the number of pipes of hydraulic radius R_h, dimensionless; q_h, flow rate of single pipe, $m^3 \cdot s^{-1}$; ϕ, porosity, dimensionless; A_b, bulk surface area of porous media normal to flow direction, m^2; R_h, hydraulic radius, m)	Simple in formula and easy for calculation	Negligence of pore structure, e.g., different pore shapes, pore connectivity, etc.
Integral pipe model (this chapter)	$Q = \int_{r_{in,\min}}^{r_{in,\max}} \frac{10^{18} N \phi_{co} V_{co}}{\pi {r_{in}}^3 L_{co} \sigma \sqrt{2\pi}} \cdot e^{-0.5\left(\frac{\ln r_{in} - \eta}{\sigma}\right)^2} dr_{in}$ (Q, total flow, $kg \cdot s^{-1}$; $r_{in,\max}$ and $r_{in,\min}$, the minimum and maximum values of the inner radius of pipes, nm; N, mass flow in a pipe, $kg \cdot s^{-1}$; Φ_{co}, porosity of a core sample, dimensionless; V_{co}, apparent volume of a core sample, m^3; r_{in}, inner radius of a pipe, nm; L_{co}, length of a core sample, m; σ, variance, dimensionless; η, normal mean, dimensionless)	Make the consideration of various pore sizes happen; easy for calculation	Negligence of pore structure, e.g., different pore shapes, pore connectivity, etc.
Total addition model [27]	$q = \sum_i q_i$ (q, total flow, $m^3 \cdot s^{-1}$; q_i, flow rate of the ith single pipe, $m^3 \cdot s^{-1}$)	Consider the flow rate in every single pipe	Impractical to implement; negligence of pore structure, e.g., different pore shapes, pore connectivity, etc.
Model of statistical sum of permeability from each shape type [49, 50]	$\left(k_{app,pm}\right)_{\text{eff}} = \left[\left(k_{app,pm}^{\frac{x}{100}}\right)_{\text{slit}} \times \left(k_{app,pm}^{1-\frac{x}{100}}\right)_{\text{tube}}\right]$ ($k_{app,pm}$, apparent permeability modified for ultratight porous media, m^2; $x/100$, percentage of rectangular slits pores; $(1-x/100)$, percentage of cylindrical pores)	Pore shapes, i.e., rectangular slits and cylindrical tubes, are taken into account	The quantification of the percentages of different pore types using image analysis tools is hard to implement; negligence of various pore sizes
3D fractal model [51]	Please refer to Eqs. (24)–(27) in literature [51] for the specific expressions where the formulas are complex	Multi-scale pore size distribution and tortuous flow line in 3D space of shale matrix are characterized	Many parameters to be determined; negligence of different pore shapes
Homogenization model [52, 53]	The homogenization method is used to upscale gas flow through two distinct constituents, a mineral matrix and organic matter. A gas flow in a two-constituent composite	The constituents, i.e., mineral matrix and organic matter, in shale are taken into account	Multiple assumptions; redundant processing for model establishment and solution

Method	Description/equation	Advantages	Shortcomings
	porous medium is considered, in which a microscopic unit cell is periodically repeated		
Pore network model [54, 55]	Generate pore network models by extracting pore structure information from real images or generate porous media by simulating the sedimentation and diagenesis processes and then incorporate relevant flow mechanisms into the gas flow models	Pore size distribution, anisotropy and low connectivity of the pore structure, etc. can be taken into account	Substantial work for model establishment; representativeness and verisimilitude of pore network models to the real pore structures remain a challenge

Table 3.
Comparison of upscaling methods from microscopic to macroscopic scale.

Method (3): the statistical sum method of the individual permeability from each shape type [49, 50].

Method (4): the 3D fractal model with variable pore sizes [51].

Method (5): the homogenization method to upscale gas flow through two distinct constituents, a mineral matrix and organic matter [52, 53].

Method (6): the pore network model including pore size distribution, anisotropy, and low connectivity of the pore structure, etc. in shale [54, 55].

The comparison among them is summarized in **Table 3**.

After reviewing the upscaling methods in **Table 3**, it is obvious that the method used in this work is not a bad compromise when compared to method (1) which is too simple and coarse, methods (2) and (3) where it is impractical and daunting to count the size/shape of every single pore with huge computational efforts, method (5) where complex processing for the model establishment and solution is needed, and methods (4) and (6) where redundant parameters/information about pore structure need to be assumed or obtained from multiple ways. Therefore, on the one hand, only the pore size distribution experiment is needed for the determination of the upscaling parameters in this chapter to make the consideration of various pore sizes happen. On the other hand, the derived model in this chapter is practical to operate, and the results can thus be readily obtained. However, it does not necessarily mean that there is no drawback for the upscaling method used. For example, although SEM images of the shale samples show that the pores in the organic matter are mostly circular [56], various types of pore shapes, e.g., cylindrical, triangular, rectangular shaped, etc., can be detected in shale samples [50, 57]. Singh et al. [50] concluded that the geometry of pores significantly influences apparent permeability of shale and diffusive flux. The study of effective liquid permeability in a shale system by Afsharpoor and Javadpour [58] confirmed that the assumption of simplified circular pore causes apparent permeability to be significantly overestimated and the discrepancy between the realistic multi-geometry pore model and the simplified circular pore model becomes more pronounced when pore sizes reduce and liquid slip on the inner pore wall is taken into account. Xu et al. [59] developed a model for gas transport in tapered noncircular nanopores of shale rocks and found the following: (1) pore proximity induces faster gas transport, and omitting pore proximity leads to the enlargement of the adsorbed gas-dominated region; (2) increasing taper ratio (ratio of inlet size to outlet size) and aspect ratio weakens real gas effect and lowers free gas transport; (3) moreover, it lowers the total transport capacity of the nanopore, and the tapered circular nanopore owns the greatest

transport capacity, followed by tapered square, elliptical, and rectangular nanopores. To conclude, there is still much room for improvement of the upscaling method in this work in multiple aspects in future research.

5. Translation of lab-scale results into field-scale ones

With the properties of multi-scale pore structures and various reservoir modes, the shale gas reservoir is complex in reservoir space and occurrence modes, which in turn leads to different flow mechanisms in multi-scale spaces. Therefore, adopting single-scale equations and flow simulation methods will not accurately reveal the flow mechanism in complex shale gas reservoirs [60]. Jiao et al. [61] established an effective conversion relation between physical simulation parameters and field parameters based on similarity criterion to better simulate gas reservoir development. The ideas in literature [61] are narrated as follows.

First, considering the flow mechanism of shale gas in the reservoir, the selected characteristic physical parameters are permeability K, porosity ϕ, pore radius r, length L, original pressure p_i, flow rate of gas production q, gas compression factor Z, reservoir temperature T, standard temperature T_{sc}, and standard atmospheric pressure p_{sc}. According to the π theory, there are four basic dimensions named length dimension [L], mass dimension [M], time dimension [T], and temperature dimension [K]. Therefore, each of π is obtained, and field parameters are analyzed to deduce physical simulation parameters in the experiment according to the similarity criterion, as shown in **Table 4**.

Second, based on the similarity criterion, the conversion relation between physical simulation parameters and field parameters can be established, which is expressed as:

$$q_g = \frac{\pi r^2 K_{rg} K T_{sc} p_i^2}{LuZTp_{sc}} \left(\frac{LuZTp_{sc}}{\pi r^2 K_{rg} K T_{sc} p_i^2} q \right)_m \tag{10}$$

where m indicates that the parameters inside the brackets are for the physical simulation.

Finally, choose the core sample "Ning 211-1" for an example to conduct dynamic physical experiment under different conditions, which is used to verify the

Number	Similarity criterion	Similar attributes	Physical significance	Value of physical simulation	Actual value of reservoir
1	$\pi_1 = \phi$	Porosity similarity	Determine porosity	0.02–0.2	0.02–0.2
2	$\pi_2 = Z$	Compression similarity	Determine model gas	0.9–1.2	0.9–1.2
3	$\pi_3 = T/T_{SC}$	Temperature similarity	Determine model temperature	1–1.1	1.1–1.3
4	$\pi_4 = r/L$	Geometric similarity	Determine model size	0.3–1	0.3–1
5	$\pi_5 = p_{sc}/p_i$	Dynamic similarity	Determine original pressure of model	0.002–0.01	0.002–0.005
6	$\pi_6 = p_w/p_i$	Dynamic similarity	Determine conversion relation for bottom hole pressure	0–1.0	0.1–1.0
7	$\pi_7 = \frac{qLuZTp_{SC}}{\pi r^2 K K_g T_{SC} p_i^2}$	Movement similarity	Determine production rate	0–0.5	0.1–0.3

Table 4.
Similarity criterion numerals of the gas reservoir physical simulation.

T_{sc}/K	293.15						
Φ_{co}	5.6%						
r_m/m	0.0127						
r/m	40						
L_m/m	0.0557						
L/m	20						
T_m/K	298.15						
T/K	353.15						
$p_i/(10^6$Pa)	3.0745	4.0995	5.0800	6.5750	7.6500	10.2300	12.5900
$u/(10^{-5}$ Pa·s)	1.1560	1.1785	1.2030	1.2461	1.2817	1.3830	1.4944
Z_m	0.9481	0.9316	0.9163	0.8942	0.8795	0.8493	0.8294
Z	0.9747	0.9670	0.9602	0.9507	0.9445	0.9326	0.9254
q_m/(ml/s)	0.0344	0.0466	0.0570	0.0746	0.0877	0.1205	0.1450
q_g/(ml/s)	785.5063	1055.4281	1278.7645	1649.5661	1919.8761	2579.8383	3055.2185
q/(ml/s)	748.2798	1021.0548	1255.2453	1601.7201	1902.6402	2529.7590	3038.9881

Table 5.
Parameters for application.

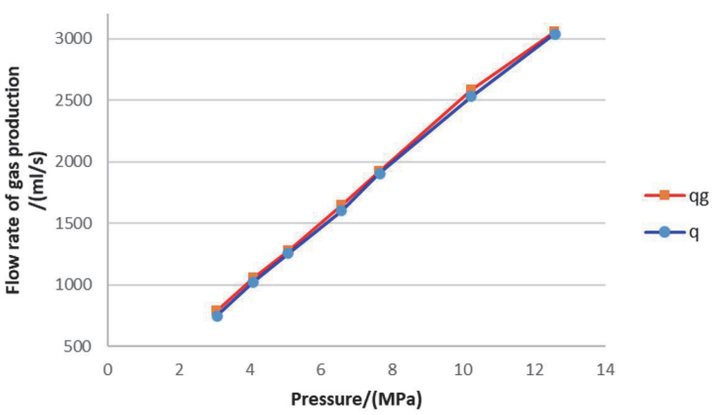

Figure 5.
Comparison of actual values of reservoir and predicted field results based on similarity conversion.

rationality of the similarity criterion. The related parameters, values of physical simulation (q_m), converted values of field (q_g), and actual values of reservoir (q) are presented in **Table 5**.

Figure 5 displays the curves of actual values of reservoir and predicted field results based on similarity conversion, the latter of which are calculated from the physical experiment. The results calculated by similarity criterion are basically consistent with the on-site tested data. It is expected that applying the similarity translation from physical simulation of gas reservoirs is capable of predicting the development performance effectively, showing the rationality of the translation method.

6. Conclusions

Based on our study in this chapter, the following conclusions have been reached:

1. A new concept "wall-associated diffusion" was introduced to the study of gas flow in shale nanopores, which has practical significance and multiple research

significance. By virtue of this concept, viscous flow, bulk diffusion, surface diffusion, and Knudsen diffusion were considered in the proposed flow mechanism scheme for nanoscale shale gas flow, with both division of mechanical mechanisms in nanopores and partition of flow space taken into account. Viscous flow and bulk diffusion belong to the bulk phase flow, which result from gas-gas interactions. In addition, surface diffusion and Knudsen diffusion are of boundary layer flow, which are associated with gas-wall interactions.

2. An easy-to-operate coupling method of the flow mechanism scheme containing four coupling coefficients and thus a coupled shale gas flow model in nanopores, which applies within the scope of full flow regimes and avoids segment processing, was proposed.

3. Based on the experimental data of pore size distributions of real shale samples from a gas field, a new coupled upscaling flow model in macroscopic-scale shale matrix with the experimentally determined fitting parameters was established. The model uses smooth functions to fit the full-scale pore size distribution results to facilitate the upscaling transformation of the model in nanopores into that in the macroscopic matrix.

4. A case study was presented to show how the lab-scale results are translated into field-scale ones, revealing the rationality of the translation method used.

In summary, sounder in theoretical bases and better in application effects, the proposed model is expected to be of practical significance for evaluating the gas flow capacity in shale matrix and guiding gas reservoir development in gas fields.

Acknowledgements

This work was supported by the National Science and Technology Major Project of the Ministry of Science and Technology of China (grant number 2017ZX05037 – 001); the Demonstration Project of the National Science and Technology Major Project of the Ministry of Science and Technology of China (grant number 2016ZX05062 – 002 – 001); and the Science and Technology Major Project of PetroChina (grant number 2016E–0611).

Author details

Zhiming Hu[1], Yaxiong Li[2*] and Yanran Li[1,3,4]

1 Research Institute of Petroleum Exploration and Development, China National Petroleum Corporation, Langfang, People's Republic of China

2 SINOPEC Petroleum Exploration and Production Research Institute, Beijing, People's Republic of China

3 University of Chinese Academy of Sciences, Beijing, People's Republic of China

4 Institute of Porous Flow and Fluid Mechanics, Chinese Academy of Sciences, Langfang, People's Republic of China

*Address all correspondence to: liyaxiong.syky@sinopec.com

References

[1] Zhang et al. Foundation of Shale Gas Reservoir Development. 1st Ed. Beijing: Petroleum Industry Press; 2014

[2] Klinkenberg LJ. The Permeability of Porous Media to Liquid and Gases. In: API 11th Mid Year Meeting, May, Tulsa, USA

[3] Javadpour F. Nanopores and apparent permeability of gas flow in mudrocks (shales and siltstone). Journal of Canadian Petroleum Technology. 2009;**48**(08):16-21. DOI: 10.2118/09-08-16-DA

[4] Haghshenas B, Clarkson C R, Chen S. Multi-porosity multi-permeability models for shale gas reservoirs. In: SPE Unconventional Resources Conference Canada. Society of Petroleum Engineers; 2013

[5] Wu K, Li X, Wang C, et al. A model for gas transport in microfractures of shale and tight gas reservoirs. AICHE Journal. 2015;**61**(6):2079-2088. DOI: 10.1002/aic.14791

[6] Sun F, Yao Y, Li G, et al. A slip-flow model for multi-component shale gas transport in organic nanopores. Arabian Journal of Geosciences. 2019;**12**:143. DOI: 10.1007/s12517-019-4303-6

[7] Veltzke T, Thöming J. An analytically predictive model for moderately rarefied gas flow. Journal of Fluid Mechanics. 2012;**698**:406-422. DOI: 10.1017/jfm.2012.98

[8] Li Y, Li X, Shi J, et al. A nano-pore scale gas flow model for shale gas reservoir. In: SPE Energy Resources Conference. Society of Petroleum Engineers; 2014

[9] Mi L, Jiang H, Li J. The impact of diffusion type on multiscale discrete fracture model numerical simulation for shale gas. Journal of Natural Gas Science and Engineering. 2014;**20**:74-81. DOI: 10.1016/j.jngse.2014.06.013

[10] Song W, Yao J, Li Y, et al. Apparent gas permeability in an organic-rich shale reservoir. Fuel. 2016;**181**:973-984. DOI: 10.1016/j.fuel.2016.05.011

[11] Beskok A, Karniadakis GE. Report: A model for flows in channels, pipes, and ducts at micro and nano scales. Microscale Thermophysical Engineering. 1999;**3**(1):43-77

[12] Civan F. Effective correlation of apparent gas permeability in tight porous media. Transport in Porous Media. 2010;**82**(2):375-384. DOI: 10.1007/s11242-009-9432-z

[13] Moridis GJ, Blasingame TA, Freeman CM. Analysis of mechanisms of flow in fractured tight-gas and shale-gas reservoirs. In: SPE Latin American and Caribbean Petroleum Engineering Conference. Society of Petroleum Engineers; 2010

[14] Freeman CM, Moridis GJ, Blasingame TA. A numerical study of microscale flow behavior in tight gas and shale gas reservoir systems. Transport in Porous Media. 2011;**90**(1): 253-268. DOI: 10.1007/s11242-011-9761-6

[15] Michel GG, Sigal RF, Civan F, et al. Parametric investigation of shale gas production considering nano-scale pore size distribution, formation factor, and non-Darcy flow mechanisms. Society of Petroleum Engineers. 2011;**147438**: 38-46. DOI: 10.2118/147438-MS

[16] Deng J, Zhu W, Ma Q. A new seepage model for shale gas reservoir and productivity analysis of fractured well. Fuel. 2014;**124**:232-240. DOI: 10.1016/j.fuel.2014.02.001

[17] Deng J, Zhu W, Qi Q, et al. Study on the steady and transient pressure

characteristics of shale gas reservoirs. Journal of Natural Gas Science and Engineering. 2015;**24**:210-216. DOI: 10.1016/j.jngse.2015.03.016

[18] Roy S, Raju R, Chuang HF, et al. Modeling gas flow through microchannels and nanopores. Journal of Applied Physics. 2003;**93**(8): 4870-4879. DOI: 10.1063/1.1559936

[19] Tang GH, Tao WQ, He YL. Gas slippage effect on microscale porous flow using the lattice Boltzmann method. Physical Review E. 2005;**72**(5): 056301. DOI: 10.1103/PhysRevE.72.056301

[20] Javadpour F, Fisher D, Unsworth M. Nanoscale gas flow in shale gas sediments. Journal of Canadian Petroleum Technology. 2007;**46**(10): 55-61. DOI: 10.2118/07-10-06

[21] Swami V, Settari A. A pore scale gas flow model for shale gas reservoir. In: SPE Americas Unconventional Resources Conference. Society of Petroleum Engineers; 2012

[22] Ziarani AS, Aguilera R. Knudsen's permeability correction for tight porous media. Transport in Porous Media. 2012; **91**(1):239-260. DOI: 10.1007/s11242-011-9842-6

[23] Veltzke T, Thöming J. An analytically predictive model for moderately rarefied gas flow. Journal of Fluid Mechanics. 2012;**698**:406-422. DOI: 10.1017/jfm.2012.98

[24] Wu L. A slip model for rarefied gas flows at arbitrary Knudsen number. Applied Physics Letters. 2008;**93**(25):253103. DOI: 10.1063/1.3052923

[25] Singh H, Javadpour F. Langmuir slip-Langmuir sorption permeability model of shale. Fuel. 2016;**164**:28-37. DOI: 10.1016/j.fuel.2015.09.073

[26] Zhang P, Hu L, Meegoda JN. Pore-scale simulation and sensitivity analysis of apparent gas permeability in shale matrix. Materials. 2017;**10**(2):104. DOI: 10.3390/ma10020104

[27] Kuila U, Prasad M, Kazemi H. Application of Knudsen flow in modeling gas–flow in shale reservoirs. In: 9th Biennial International Conference and Exposition on Petroleum Geophysics, Hyderabad, India; 2013

[28] Dongari N, Sharma A, Durst F. Pressure-driven diffusive gas flows in micro-channels: From the Knudsen to the continuum regimes. Microfluidics and Nanofluidics. 2009;**6**(5):679-692. DOI: 10.1007/s10404-008-0344-y

[29] Rahmanian M, Aguilera R, Kantzas A. A new unified diffusion–viscous-flow model based on pore-level studies of tight gas formations. SPE Journal. 2012;**18**(01): 38-49. DOI: 10.2118/149223-PA

[30] Wu K, Chen Z, Wang H, et al. A model for real gas transfer in nanopores of shale gas reservoirs. Society of Petroleum Engineers. 2015. DOI: 10.2118/174293-MS

[31] Geng L, Li G, Zitha P, et al. A diffusion–viscous flow model for simulating shale gas transport in nano-pores. Fuel. 2016;**181**:887-894. DOI: 10.1016/j.fuel.2016.05.036

[32] Sun F, Yao Y, Li G, et al. Transport behaviors of real gas mixture through nanopores of shale reservoir. Journal of Petroleum Science and Engineering. 2019;**177**:1134-1141. DOI: 10.1016/j.petrol.2018.12.058

[33] Klinkenberg LJ. The Permeability of Porous Media to Liquids and Gases. In: API 11th Mid Year Meeting. American Petroleum Institute; 1941

[34] Hongkui G, Shen Y, Yan S, et al. Slippage effect of shale gas flow in

nanoscale pores. Natural Gas Industry. 2014;**34**(7):46-54. DOI: 10.3787/j.issn.1000-0976.2014.07.008

[35] Zhu Y, Xiangui L, Tieshu L, et al. A study of slippage effect of gas percolation in low permeability gas pools. Natural Gas Industry. 2007;**27**(5): 44-47

[36] Daixun C. Gas slippage phenomenon and change of permeability when gas flows in tight porous media. Acta Mech. Sin. 2002; **34**(1):96-100

[37] KeLiu WU, XiangFang LI, ZhangXing CHEN. The mechanism and mathematical model for the adsorbed gas surface diffusion in nanopores of shale gas reservoirs. Science China Press. 2015;**45**(5):525-540. DOI: 10.1360/N092014-00263

[38] Baisheng N, Li Z, Ma W. Diffusion micro-mechanism of coal bed methane in coal pores. Coal Geology & Exploration. 2000;**28**(6):20-22

[39] Lidong M, Hanqiao J, Junjian L, Ye T. Mathematical characterization of permeability in shale reservoirs. Acta Petrolei Sinica|Acta Petrol Sin. 2014; **35**(5):928-934. DOI: 10.7623/syxb201405013

[40] Li Y, Liu X, Hu Z, et al. A new method for the transport mechanism coupling of shale gas slippage and diffusion. Acta Physica Sinica. 2017;**66**: 114702. DOI: 10.7498/aps.66.114702

[41] Li Y, Hu Z, Duan X, et al. The general form of transport diffusivity of shale gas in organic-rich nano-slits—A molecular simulation study using darken approximation. Fuel. 2019;**249**: 457-471. DOI: 10.1016/j.fuel.2019.03.074

[42] Li Y, Liu X, Gao S, et al. A generalized model for gas flow prediction in shale matrix with deduced coupling coefficients and its macroscopic form based on real shale pore size distribution experiments. Journal of Petroleum Science and Engineering. 2019;**187**:106712. DOI: 10.1016/j.petrol.2019.106712

[43] Dongari et al. Pressure−driven diffusive gas flows in micro−channels: From the Knudsen to the continuum regimes. Microfluidics and Nanofluidics. 2009;**6**:679-692. DOI: 10.1007/s10404-008-0344-y

[44] Wu K, Chen Z, Li X, et al. Flow behavior of gas confined in nanoporous shale at high pressure: Real gas effect. Fuel. 2017;**205**:173-183. DOI: 10.1016/j.fuel.2017.05.055

[45] Niu et al. Second−order gas−permeability correlation of shale during slip flow. SPE Journal. 2014;**19**: 786-792. DOI: 10.2118/168226-PA

[46] Chen et al. Channel−width dependent pressure−driven flow characteristics of shale gas in nanopores. AIP Advances. 2017;**7**:045217. DOI: 10.1063/1.4982729

[47] Xiong X, Devegowda D, Villazon M, et al. A fully-coupled free and adsorptive phase transport model for shale gas reservoirs including non-Darcy flow effects. SPE annual technical conference and exhibition. Society of Petroleum Engineers; 2012

[48] Etminan SR, Javadpour F, Maini BB, et al. Measurement of gas storage processes in shale and of the molecular diffusion coefficient in kerogen. International Journal of Coal Geology. 2014;**123**:10-19. DOI: 10.1016/j.coal.2013.10.007

[49] Fenton L. The sum of log-normal probability distributions in scatter transmission systems. IRE Transactions on Communication Systems. 1960;**8**: 57-67

[50] Singh H, Javadpour F, Ettehadtavakkol A, Darabi H. Nonempirical apparent permeability of shale. SPE Reservoir Evaluation and Engineering. 2014;**17**:414-424. DOI: 10.2118/170243-PA

[51] Cai J, Lin D, Singh H, Wei W, Zhou S. Shale gas transport model in 3D fractal porous media with variable pore sizes. Marine and Petroleum Geology. 2018;**98**:437-447. DOI: 10.1016/j.marpetgeo.2018.08.040

[52] Auriault JL. Heterogeneous medium. Is an equivalent macroscopic description possible? International Journal of Engineering Science. 1991;**29**: 785-795. DOI: 10.1016/0020-7225(91)90001-J

[53] Darabi H, Ettehad A, Javadpour F, Sepehrnoori K. Gas flow in ultra-tight shale strata. Journal of Fluid Mechanics. 2012;**710**:641-658. DOI: 10.1016/0020-7225(91)90001-J

[54] Zhang P, Hu L, Meegoda J. Pore-scale simulation and sensitivity analysis of apparent gas permeability in shale matrix. Materials. 2017;**10**:104. DOI: 10.3390/ma10020104

[55] Wang L, Wang S, Zhang R, Wang C. Review of multi-scale and multi-physical simulation technologies for shale and tight gas reservoirs. Journal of Natural Gas Science and Engineering. 2017;**37**:560-578. DOI: 10.1016/j.jngse.2016.11.051

[56] Javadpour F, McClure M, Naraghi ME. Slip-corrected liquid permeability and its effect on hydraulic fracturing and fluid loss in shale. Fuel. 2005;**160**:549-559. DOI: 10.1016/j.fuel.2015.08.017

[57] Song W, Yao J, Ma J, Li A, Li Y, Sun H. Grand canonical Monte Carlo simulations of pore structure influence on methane adsorption in micro-porous carbons with applications to coal and shale systems. Fuel. 2018;**215**:196-203. DOI: 10.1016/j.fuel.2017.11.016

[58] Afsharpoor A, Javadpour F. Liquid slip flow in a network of shale noncircular nanopores. Fuel. 2016;**180**: 580-590. DOI: 10.1016/j.fuel.2016.04.078

[59] Xu J, Wu K, Yang S, Cao J, Chen Z, Pan Y, et al. Real gas transport in tapered noncircular nanopores of shale rocks. AICHE Journal. 2017;**63**: 3224-3242. DOI: 10.1002/aic.15678

[60] Sun H, Yao J, Yalchin E. Upscaling of gas transport in shale matrix based on homogenization theory(in Chinese). Science China Physics, Mechanics & Astronomy. 2017;**47**:114612. DOI: 10.1360/SSPMA2016-00531

[61] Chunyan JIAO, Huaxun LIU, Pengfei LIU, et al. Similarity criterion of the physical simulating experiment for the development performances of low-permeability tight gas reservoirs. Petroleum Geology and Oilfield Development in Daqing. 2019;**38**(1): 155-161